Madras Journal Series Pvt Ltd
Advanced Materials & Applications
Adv. Mater. App. 5 (2020) 24-30
ISSN: 2582-5070

Synthesis and characterization of binary composite $ZrO_2/ZnCo_2O_4$ thin films

A. Kharroubi[1,*], A. Khiali[1], H. Benhebal[2], S. Hamdi[1], B. Benrabah[1]

[1]Laboratory of Physical Engineering, University of Tiaret, Algeria.

[2]Department of Chemical, Faculty of Mater Sciences, University of Tiaret, Algeria.

***Corresponding author:** kharoubilmd@hotmail.fr

Received 24 January 2020, Received in final form 07 February 2020, Accepted 08 February 2020

Abstract

$ZnCo_2O_4$ and $ZrO_2/ZnCo_2O_4$ composite thin films with (5%, 10%, 15%, 20%) wt ZrO_2 are deposited by the dip-coating technique on glass substrates and silicon substrates. Structural, optical and electronic properties of synthesized materials were characterized by ultra-violet-visible spectroscopy (UV-visible), X-ray diffraction, Fourier transform infrared spectroscopy and complex impedance spectroscopy. The X-ray diffraction patterns show the spinel structure of $ZnCo_2O_4$ with a preferential orientation according to (311). The average grain size of the samples varies from 19.4 to 16.8 nm. Infrared transmission spectra show bands 400 cm^{-1} and 800 cm^{-1} are attributed to M-O skeletal vibration of mixed oxides. All films exhibit high transparency (80%) over the visible range. The optical bandgap decreases from 3.62 eV to 3.521 eV due to the extent of electronic states introduced by ZrO_2 incorporation. The impedance measurements show that the equivalent circuit of the diagram of $ZnCo_2O_4$ films is an R_pC_p parallel .The resistance R_P decreases while the capacitance C_P increases with ZrO_2-doping.

Keywords: *$ZnCo_2O_4$, ZrO_2, thin films, Sol-gel, Dip-coating.*

1. Introduction

$ZnCo_2O_4$ has attracted much attention in recent years due to its unique magnetic and electrical properties and chemical stability. These properties are important not only from a fundamental point of view, for example ferromagnetism [1]; and the ability to control carrier types through the oxygen growth atmosphere[2], but also for their potential applications, such as semiconductor magnetic dilution, spin electronics, optoelectronics, hollow structures [3], mesoporous structures [4], and anode material [5]. Its crystalline structure is a spinel with Zn^{2+} occupying the tetrahedral sites and Co^{3+} occupying the octahedral sites. Various methods, including physical and chemical techniques, were used to prepare thin film, nanoscale and thin film $ZnCo_2O_4$. Most of the reported work focused on p-$ZnCo_2O_4$ growth and characterization of their electrical and magnetic properties [6]. Few works have studied the heterostructures of $ZnCo_2O_4$ [7], but $ZnCo_2O_4$'s thin films remain potential candidates for several applications [8]. The stoichiometry of the different chemical elements can be easily controlled by mixing the different precursors in the initial solution. Low viscosity (in general) provides good molecular homogeneity [9].

2. Materials and methods

2.1. Preparation of $ZrO_2/ZnCo_2O_4$ composite

$ZnCo_2O_4$ solutions are obtained by mixing two types of preparations. The first preparation is obtained by dissolving 2.11 g of Zinc nitrate hexahydrate ($Zn(NO_3)_2.6H_2O$) in 20 ml of ethanol. Magnetic agitation for 10 minutes leads to the formation of a colorless solution. The second is an ethanoic solution of cobalt nitrates obtained by dissolving 4.70 g cobalt nitrates hexahydrate ($Co(NO_3)_2,6H_2O$) in 30 ml ethyl alcohol. After mixing the two preparations, an ethanolic solution of oxalic acid, which is prepared by dissolving 0.7g $C_2H_2O_4$ in 50 ml of ethanol, is added drop by drop. The mixture is heated slowly at 80°C for 2 h under magnetic agitation this solution is characterized by a dark violet color.

$ZrO_2/ZnCo_2O_4$ solutions were prepared using 5 ml of 70wt% zirconium propoxide $Zr(OCH(CH_3)_2)_4$ as precursor dissolved in 10 ml of isopropanol ($CH_3CHOHCH_3$) under stirring for 10 min. Then 3 ml of acetylacetone ($C_5H_8O_2$) and 50ml of isopropanol ($CH_3CHOHCH_3$) were added to the above solution under stirring for 1 h. The solution obtained is transparent, yellowish in color and slightly viscous (Fig. 1). Pyrex substrates of 25×75×1.75 mm^3

© 2020 Madras Journal Series Pvt Ltd

were cleaned with distilled water, acetone and ethanol respectively for 15 min using an ultrasonic bath and then, dried at 100°C in air. The films were then deposited by dip-coating at a drawing speed of 50 mm/min.

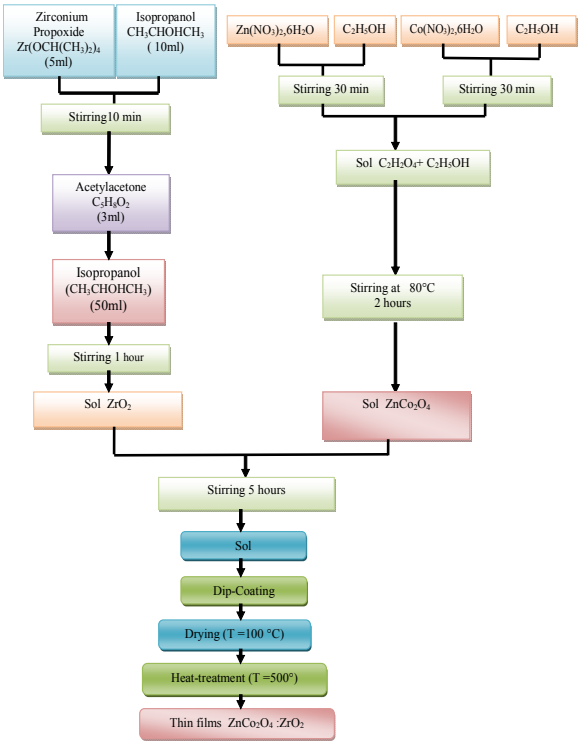

Fig. 1. *Schematic diagram of sol–gel synthesis of $ZrO_2/ZnCo_2O_4$.*

2.2. Characterization

The crystal phase and the crystallite size of $ZnCo_2O_4$ and $ZrO_2/ZnCo_2O_4$ composite were determined by X-ray diffraction (XRD) using Rigaku MINIFLEX 600 with Cu.K_α (λ=1.5406Å) X-ray diffractometer. The optical transmittance of the films was measured using UV-1650 Shimadzu spectrophotometer in the wavelength range from 300nm to900 nm. FTIR spectra of the samples were recorded using a Shimadzu 8400 spectrometer in the wave number range from 400 cm^{-1} to 4000 cm^{-1}. Impedance measurements were carried out using an Agilent 4284A LCR-meter operating in the range of 75 KHz-1MHz with oscillation amplitude of 1V.

3. Results and discussion

3.1. X-ray diffraction studies

Fig. 2 shows the X-ray diffraction patterns of $ZnCo_2O_4$ and $ZrO_2/ZnCo_2O_4$ samples annealed at 450°C for 2 h. All reflections can be indexed to the $ZnCo_2O_4$ (JCPDS #23-1390) centered cubic with $ZnCo_2O_4$ spinel structure with preferential orientation according to (311) [10]: The phase has been shown on the diffractograms display the characteristic diffraction angles at 18.77°, 31.14°, 36.74°, 40.6°, 44.57°, 55.49°, 59.08°, 65.17°, 75.12°, 77.32° and 79.43° correspond to the planes (111), (220), (311), (222), (400), (422), (511), (440) (620), (533) and (622) respectively. Additional diffraction peaks of the tetragonal structure of zirconium oxide are detected at 2θ equal to 30.02° and 35.2° corresponding to the crystal planes (111) and (200) [11,12].

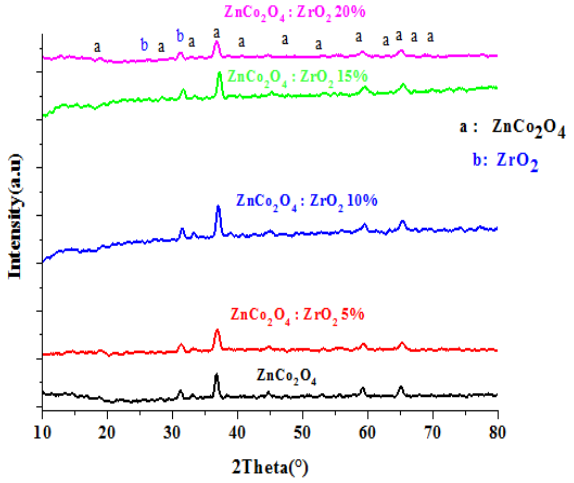

Fig. 2. *XRD patterns of $ZnCo_2O_4$ and $ZrO_2/ZnCo_2O_4$ samples*

The average crystallite sizes are calculated at half-maximum intensity using Debye–Scherrer formula [13].

$$D = \frac{0.9\lambda}{\beta\cos\theta} \quad (1)$$

Where D is the grain size, λ is the wavelength of the X-ray radiation ($\lambda_{Cu\text{-}K\alpha}$ = 1.541874 Å), β is the full width at half maximum (FWHM) and θ is the Bragg angle. Table 1 summarizes the structural parameters.

Table 1. *Crystallite sizes of undoped and ZrO_2-doped $ZnCo_2O_4$.*

Samples	2θ	FWHM	D	B(rd)	τ (Å)
0%	36.69	0.43	2.44	0.0075	19.49
5%	36.741	0.42	2.44	0.0073	20.02
10%	36.869	0.56	2.43	0.0097	15.07
15%	37.11	0.54	2.54	0.0094	15.57
20%	36.67	0.50	2.44	0.0087	16.80

From Table 1, it is observed that the crystallite size of materials decreases (from 19.49 to 16.80 nm) when the ZrO_2 amount increases (from 0

© 2020 Madras Journal Series Pvt Ltd

to 20 wt %). The introduction of ZrO_2 into the $ZnCo_2O_4$ matrix probably disrupts crystallization and slows the growth rates of crystals as observed in later studies [14].

3.2. FT-IR spectroscopy

FTIR spectra of thin films are shown in Fig. 3. The bands between 400 cm^{-1} and 800cm^{-1} are attributed to M-O vibration skeletal mixed oxides. In particular, the 483 cm^{-1} band is the characteristic peak of ZnO and 680 cm^{-1} (ν_1), 582 cm^{-1} (ν_2) are derived from the M-O stretching vibration modes for tetrahedral coordination of Zn and Co-O ions for octahedral Co, respectively, which confirms the formation of the spinel structure characteristic peaks of the $ZnCo_2O_4$ phase [15-16].Two wide bands at 3434 cm^{-1} and 1634 cm^{-1} appeared due to O-H stretching and bending frequencies, respectively, mainly due to the presence of water molecules in the samples[17]. The peak at 2343 cm ^{1} is attributed to the vibration of absorbed CO_2 from the ambient air [18].

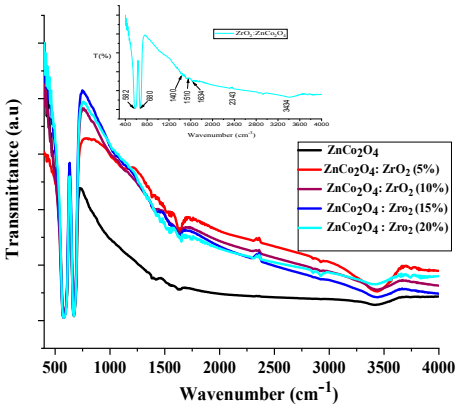

Fig. 3. *FT-IR spectra of $ZnCo_2O_4$ and $ZrO_2/ZnCo_2O_4$ films*

3.3. UV–Visible spectroscopy

Fig. 4 shows transmission spectra of the $ZnCo_2O_4$ and $ZrO_2/ZnCo_2O_4$ films. The transmission spectra have a general shape characterized by the presence of two distinct regions. We note that the films have a good transparency in the visible 75-90%, which varies slightly with zirconium oxide doping. This indicates a good optical quality of the deposited layers and shows a negligible effect of light diffusion and/or losses due to absorption. The first region shows a high transmittance with an average transmission over transparency over a wide range of wavelengths from 400 to 900 nm. This high transparency is one of the properties that explain the interest in thin layers of $ZnCo_2O_4$ as a transparent conductive material.

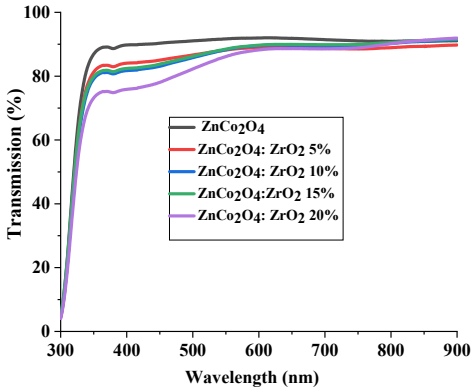

Fig. 4 *UV–visible spectra of $ZnCo_2O_4$ and $ZrO_2/ZnCo_2O_4$ films*

In the second region 300-400nm, the transmittance decreases due to absorption by the inter-band electronic transitions. A region of high absorption (λ=350 nm), which is due to the absorption of radiation by the free load carriers in the film, through inter-band electronic transitions. The transmission variation in this region is used to determine the optical gap. This region of strong absorption is exploited to determine the optical band gap (E_g) using Tauc formula [19]

$$(\alpha h\upsilon)^m = A\left(h\upsilon - E_g\right) \quad (2)$$

Where A is a constant, hν is the photon energy and m = 2 for direct allowed electronic transition. The bandgap energy of the different samples was obtained by extrapolation from the graphs of Fig. 5, representing $(h\nu)^2$ versus energy (eV).

Fig. 6 shows the variation in the Eg optical gap as a function of the ZrO_2 incorporation rate. Based on the rate of these spectra, the optical gap of the $ZnCo_2O_4$ layers decreases with the increase of the ZrO_2 doping rate from 3.62 eV for the undoped up to 3.51 eV for the sample with 20% of ZrO_2, This is mainly due to distortions in the network caused by the introduction of impurities and the increase in the concentration of free electrons.

Refractive index and porosity of the prepared films are also calculated (Table 2) respectively by the means of the following relations (Eqs. (3) and (4) [20-21]:

$$n^2 = \frac{3}{\sqrt{\frac{E_g}{20}}} \quad 2 \quad (3)$$

$$P\% = \left(1 \quad \frac{n^2 \quad 1}{n_a^2 \quad 1}\right) \times 100(\%) \quad (4)$$

© 2020 Madras Journal Series Pvt Ltd

Where n is refractive index of the film, n_d is refractive index of free-pore matrix (n_d = 2.8) and P is porosity % [22].

Table 2 resumes the values of the optical gap, refractive index and porosity of the samples $ZnCo_2O_4$. These results show that the increase of zirconium oxide doping concentration leads to an increase of the refractive index and decrease in the porosity, of the film, which can be justified by the crystallization and the densification of the material. It indicates the removal of pores and the densification of the associated film as well as the removal of organic compounds [23-26].

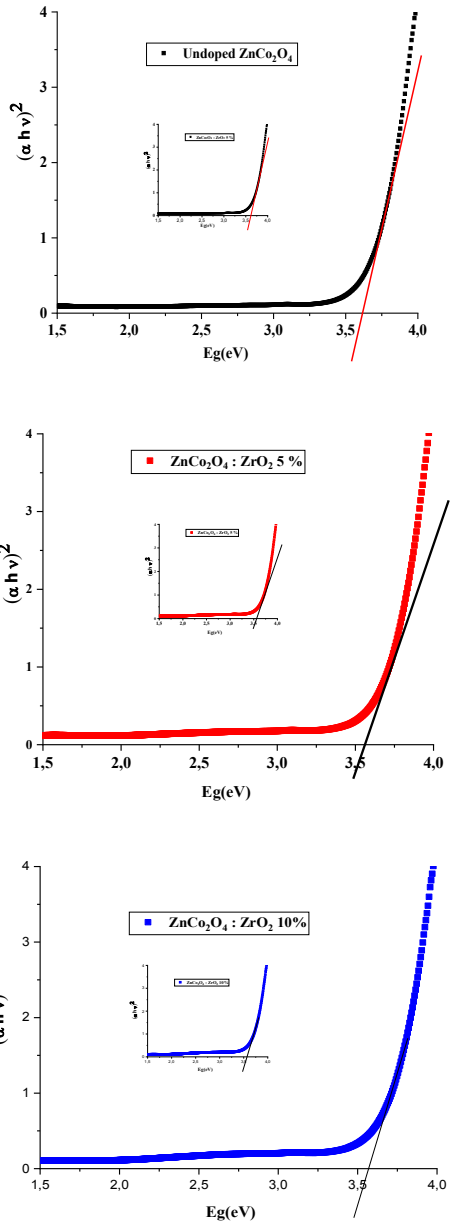

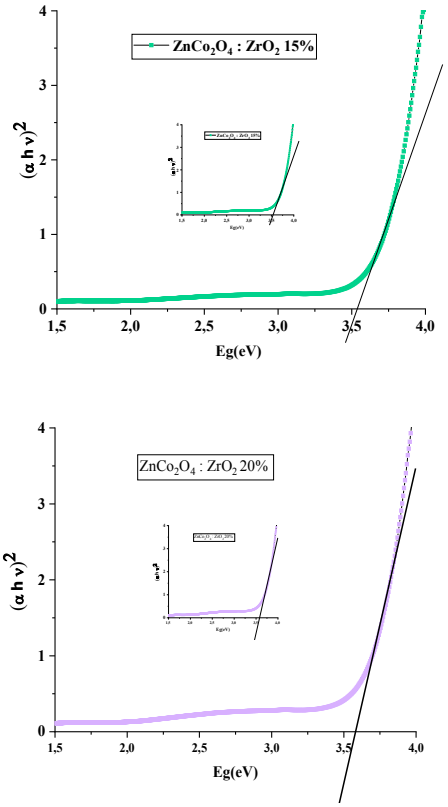

Fig. 5. *Plot of (αhν)² versus hν of $ZnCo_2O_4$ and $ZrO_2/ZnCo_2O_4$ films*

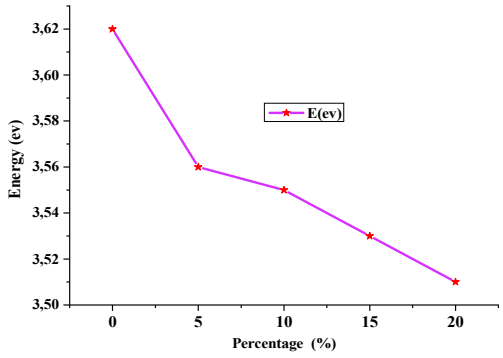

Fig. 6. *Variation of the optical gap of of $ZnCo_2O_4$ and $ZrO_2/ZnCo_2O_4$ films*

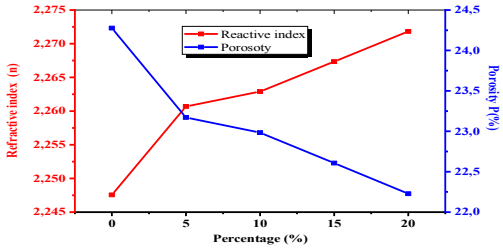

Fig. 7. *Values of n and P of $ZnCo_2O_4$ and $ZrO_2/ZnCo_2O_4$films.*

© 2020 Madras Journal Series Pvt Ltd

Table 2. *Values of the optical gap, refractive index and porosity of $ZnCo_2O_4$ and $ZrO_2/ZnCo_2O_4$ films*

Samples	Gap (eV)	Refractive Index(*n*)	Porosity *P(%)*
$ZnCo_2O_4$	3.62	2.247	24.276
$ZnCo_2O_4$: ZrO_2 (5%)	3.56	2.260	23.170
$ZnCo_2O_4$: ZrO_2 (10%)	3.55	2.2628	22.983
$ZnCo_2O_4$: ZrO_2 (15%)	3.53	2.267	22.607
$ZnCo_2O_4$: ZrO_2 (20%)	3.51	2.271	22.227

3.4. Impedance spectroscopy

The results show that the resistance of grain joints increases as the doping rate increases. This variation is due to the introduction of defects in films, which increases the potential barrier between adjacent grains. The variation in capacity is related to the formation of oxygen gaps at the interface of these grease seals. In addition, the decrease in capacity is linked to a good crystallinity in the film. This corresponds to a denser and well crystallized film while reducing the concentration of interface defects on the grain surface. The height of the potential barrier between adjacent joints is modified.

Figure 8 shows Nyquist's presentation of the thin layers of $ZnCo_2O_4$ and $ZrO_2/ZnCo_2O_4$ doped with zirconium oxide, annealed for 1 hour.

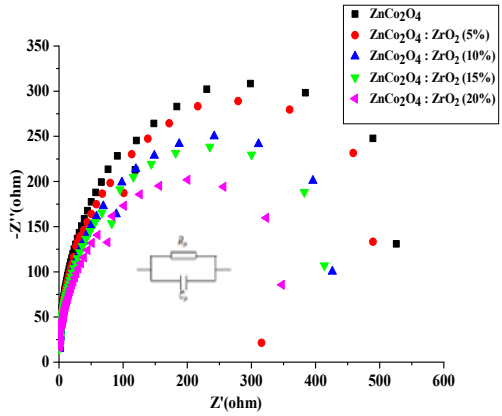

Fig. 8. *Nyquist representation of impedance data of $ZnCo_2O_4$ and $ZrO_2/ZnCo_2O_4$ films.*

The Nyquist plots suggest that the equivalent circuit is an R_pC_p parallel, where C_p is the capacitance of the layer and R_p the corresponding resistance. The capacitance of the zirconium oxide doped $ZnCo_2O_4$ samples was determined from the following equation (4):

$$C_p = \frac{1}{2\pi f_{max} R_p} \quad (4)$$

Where f_c is the frequency of the external applied field at the apex of the circular arc. The resistance R_p was determined by the intersection of the Nyquist plot with the real axis. Table 3 resumes the values of f_c, R_p, and C_p for synthesized films. The resistance decreases reaching a value of 51 Ω when the incorporation rate of ZrO_2 is increased to 20%.

Table 3. *Values of f_c, R_P and CP of $ZnCo_2O_4$ and $ZrO_2/ZnCo_2O_4$ films.*

Samples	f_c(KHz)	R_p(Ω)	C_p(nF)
Undoped $ZnCo_2O_4$	519	298	10.29
$ZnCo_2O_4$: ZrO_2 (5%)	519	278	11.03
$ZnCo_2O_4$: ZrO_2 (10%)	519	241	12.89
$ZnCo_2O_4$: ZrO_2 (15%)	519	236	13.05
$ZnCo_2O_4$: ZrO_2 (20%)	519	201	15.41

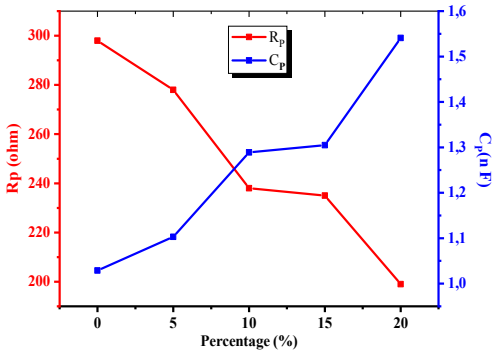

Fig. 9. *Evolution of resistance and capacitance of $ZnCo_2O_4$ and $ZrO_2/ZnCo_2O_4$ films.*

We note that the resistance of the films varies between 298 and 201 Ω, while the capacity varies between 10.29 and 15.41 nF. The increase in capacity indicates a high concentration of oxygen gaps on the grain surface, due to the substitution of Co^{2+}/Co^{3+} and Zn^{2+} ions by Zr^{3+} ions, which is a continuous path for load carriers and reduces film resistance [28]. The decrease in the thickness of the films of the samples annealed for a long time, allows one to have a good crystalline growth and the size of the crystallites gradually grows under the effect of annealing to 450°C during 1h. The number of grain joints decreases and the concentration of defects is sufficiently reduced resulting in a decrease in capacity [29].

4. Conclusion

$ZnCo_2O_4$ and $ZrO_2/ZnCo_2O_4$ thin films were synthesized by sol-gel process from the corresponding metal nitrates and deposited by dip-

© 2020 Madras Journal Series Pvt Ltd

coating technique. For the identification of the crystalline phases formed as well as the determination of the properties of the thin films produced, we used several characterization techniques, such as X-ray diffraction (DRX), optical transmission spectroscopy (UV-Visible and Infrared), complex impedance spectroscopy. The deposited layers of $ZnCo_2O_4$ and $ZrO_2/ZnCo_2O_4$ showed spinel structure of $ZnCo_2O_4$ with preferential orientation according to (311). In addition, the obtained layers show a good transmission of the order of 75 to 90% in the visible and the optical gap (E_g) varies from 3.62 eV for $ZnCo_2O_4$ undoped to 3.51 eV for $ZnCo_2O_4$:ZrO_2 (at 20%). The infrared spectra obtained for the different ZrO_2 incorporation rates show bands at 400 cm^{-1} and 800 cm^{-1}, which are attributed to M-O skeletal vibration of mixed oxides. The complex impedance spectroscopy indicates that the effect of the grain joints is dominant in the conduction mechanism; we also note that the equivalent pattern of $ZnCo_2O_4$ films for each incorporation rates is a parallel RC circuit.

Acknowledgments

The authors are thankful to the Professor Elhabib. Belarbi from the laboratory of synthesis and catalysis of Ibn-Khaldoun University for the DRX and impedance spectroscopy measurements.

References:

[1]. K. Samanta, P. Bhattacharya, R. S. Katiyar, W. Iwamoto, P. G. Pagliuso, et C. Rettori, "Raman scattering studies in dilute magnetic semiconductor $Zn_{1-x}Co_xO$", Phys. Rev. B. 73 (2006) 24.

[2]. H. J. Kim et al "Electrical and magnetic properties of spinel-type magnetic semiconductor $ZnCo_2O_4$ grown by reactive magnetron sputtering", J. Appl. Phys. 95 (2004) 11.

[3]. Liu, Mingxian, et al. "Encapsulation of NiO nanoparticles in mesoporous carbon nanospheres for advanced energy storage." Chem. Eng J. 308 (2017) 240.

[4]. Li, Yanguang, Bing Tan, and Yiying Wu. "Mesoporous Co_3O_4 nanowire arrays for lithium ion batteries with high capacity and rate capability", Nano lett. 8 (2008) 265.

[5]. Y. Sharma, N. Sharma, G. V. S. Rao, B. V. R. "Chowdari, Nanophase $ZnCo_2O4$ as a high performance anode material for Li-ion batteries", Adv. Funct. Mater. 17(2007) 2855.

[6]. N. H. Perry et T. O. Mason, "Phase Equilibria of the Zinc Oxide–Cobalt Oxide System in Air", J. Am. Ceram. Soc. 96 (2013)966.

[7]. C. Zhao et al., "Rectifying and photovoltaic properties of ZnCo2O4/Si heterostructure grown by pulsed laser deposition", Chin. Phys. B. 23. (2014) 057103.

[8]. R. Nakhowong, R. Chueachot, " Synthesis and magnetic properties of copper cobaltite ($CuCo_2O_4$) fibers by electrospinning", J. Alloys Compd. 715 (2017) 390.

[9]. A. Sarkar, K. Karmakar, G. G. Khan, "Designing Co-Pi Modified One-Dimensional n–p $TiO_2/ZnCo_2O_4$ Nano hetero structure photo-anode with reduced electron-hole Pair recombination and excellent photoconversion Effeciency (>3%)", J. Phys. Chem. C .121 (2017) 25705.

[10]. Y. Azoudj, Z. Merzougui, G. Rekhila, M. Trari, "The adsorption of $HCrO_4$ on activated carbon of date pits and its photoreduction on the hetero-system $ZnCo_2O_4/TiO_2$", App. Wat. Sci. 8 (2018) 114.

[11]. J. Rashid, M. A. Barakat, R. M. Mohamed, I. A. Ibrahim, "Enhancement of photocatalytic activity of zinc/cobalt spinel oxides by doping with ZrO2 for visible light photocatalytic degradation of 2-chlorophenol in wastewater", J. Photochem. Photobiol. A: Chem. 284 (2014) 1.

[12]. Khiali Aboulkacem, Ammari Abdelkader, Benrabah Bediaf, Bouaza Amar, Kharoubi Abdelmalek, Benhebal Hadj, "Thermally activated charge transport in modified tetragonal zirconia thin films prepared by sol–gel method"Jap. J. Appl. Phys. 57 (2017) 045801.

[13]. S. Singhal, J. Kaur, Namgyal, R. Sharma, "Cu-Doped ZnO Nanoparticles: Synthesis, Structural and Electrical Properties", Physica B. 407 (2012) 1223.

[14]. G. L. Léonard, C. M. Malengreaux, Q. Mélotte, S. D. Lambert, E. Bruneel, I. Van Driessche, B. Heinrichs, "Doped sol-gel films vs. powders TiO_2: On the positive effect induced by the

 © 2020 Madras Journal Series Pvt Ltd

presence of a substrate". J. Environ. Chem. Eng. 4 (2016) 449.

[15]. A. Alyamani, A. Tataroğlu, L. El Mir, Ahmed A. Al-Ghamdi, H. Dahman, W. A. Farooq, F. Yakuphanoğlu, "Photoresponse and photocapacitor properties of Au/AZO/p-Si/Al diode with AZO film prepared by pulsed laser deposition (PLD) method ", Appl. Phys. A, 22 (2016) 297.

[16]. G.N.Kustova, E.B.Burgina, G.G.Volkova, T.M.Yurieva, L. M. Plyasova, "IR spectroscopic investigation of cation distribution in Zn–Co oxide catalysts with spinel type structure", J. Mol. Cat. A: Chem. 158 (2000) 293.

[17]. R. Manivannan, A. Pandurangan, "Formation of ethyl benzene and styrene by side chain methylation of toluene over calcined LDHs", Appl. Clay Sci., 44 (2009) 137.

[18]. J. Jouhannaud, J. Rossignol, D. Stuerga, "Rapid synthesis of tin (IV) oxide nanoparticles by microwave induced thermohydrolysis", J. Sol. Sta. Chem. 181 (2008) 1439.

[19]. I. Saadeddin, B. Pecquenard, J. P. Manaud, R. Decourt, C. Labrugère, T. Buffeteau, and G. Campet, "Synthesis and characterization of single- and co-doped SnO_2 thin films for optoelectronic applications", Appl. Surf. Sci. 253 (2007) 5240.

[20]. J. Tian, H. Gao, H. Kong, P. Yang, W. Zhang, J. Chu, "Influence of transition metal doping on the structural, optical, and magnetic properties of TiO_2 films deposited on Si substrates by a sol-gel process", Nanoscale Res. Lett. 8 (2013) 533.

[21]. Flora Boccuzzi, Anna Chiorino, Maela Manzoli, Ping Lu, Tomoki Akita, Satosh iIchikawa, Masatake Haruta, " Au/TiO_2 nanosized samples: a catalytic, tem, and ftir study of the effect of calcination temperature on the CO oxidation", J. Catal., 202 (2001) 256.

[22]. Abdelmalek Kharoubi, Amar Bouaza, Bedhiaf Benrabah, Abdelkader Ammari, Hadj Benhebal, "Sol-Gel Dip Coating Method Synthesis of Mn-Doped Titanium Dioxide Thin Films", J. Mol. Eng. Mater. 6 (2018) 1850001.

[23]. H. Zhang, J. F. Banfield, "Size dependence of the kinetic rate constant for phase transformation in TiO_2 nanoparticles", Chem. Mater. 13 (2005) 3421-3425.

[24]. C. Suresh, V. Biju, P. Mukundan, K. G. K. Warrier, "Anatase to rutile transformation in sol-gel titania by modification of precursor", Polyhedron 17.18 (1998) 3131-3135.

[25]. Ding, Xing-zhao, Xiang-huai Liu, "Grain growth enhanced by anatase-to-rutile transformation in gel-derived nanocrystalline titania powders." J. Alloy. Comp. 248 (1997) 143.

[26]. Diebold, Ulrike, "The surface science of titanium dioxide", Surface science reports 48.5-8 (2003) 53.

[27]. C. R. Mariappan, R. Kumar, G. V. Prakash, unctional properties of $ZnCo_2O_4$ nano-particles obtained by thermal decomposition of a solution of binary metal nitrates. RSC Adv. 5 (34) 26843.

[28]. R. Muccillo, J. A. Cerri, E. R. Leite, E. Longo, J. A. Varela, "Impedance spectroscopy of SnO_2: CoO during sintering", Mater. Lett. 30 (1997) 125.

[29]. C. R. Mariappan, R. Kumar, G. V. Prakash, "Functional properties of $ZnCo_2O_4$ nano particles obtained by thermal decomposition of a solution of binary metal nitrates", RSC Adv. 5 (2015) 26843.

 © 2020 Madras Journal Series Pvt Ltd